

*Citation for published version:*

Sun, Y, Yu, F, Liao, M, Ma, J, Wang, X, He, D, Gao, W, Knight, J & Hu, L 2020, 'Visible emission and energy transfer in Tb<sup>3+</sup>/Dy<sup>3+</sup> co-doped phosphate glasses', *Journal of the American Ceramic Society*, vol. 103, no. 12, pp. 6847-6859. <https://doi.org/10.1111/jace.17391>

*DOI:*

[10.1111/jace.17391](https://doi.org/10.1111/jace.17391)

*Publication date:*

2020

*Document Version*

Peer reviewed version

[Link to publication](#)

This is the peer reviewed version of the following article: Sun, Y, Yu, F, Liao, M, et al. Visible emission and energy transfer in Tb<sup>3+</sup>/Dy<sup>3+</sup> codoped phosphate glasses. *J Am Ceram Soc.* 2020; 00: 1– 13., which has been published in final form at <https://doi.org/10.1111/jace.17391>. This article may be used for non-commercial purposes in accordance with Wiley Terms and Conditions for Self-Archiving.

**University of Bath**

## **Alternative formats**

If you require this document in an alternative format, please contact:  
[openaccess@bath.ac.uk](mailto:openaccess@bath.ac.uk)

### **General rights**

Copyright and moral rights for the publications made accessible in the public portal are retained by the authors and/or other copyright owners and it is a condition of accessing publications that users recognise and abide by the legal requirements associated with these rights.

### **Take down policy**

If you believe that this document breaches copyright please contact us providing details, and we will remove access to the work immediately and investigate your claim.

## Visible emission and energy transfer in Tb<sup>3+</sup>/Dy<sup>3+</sup> co-doped phosphate glasses

Yan Sun <sup>1,2</sup>, Fei Yu <sup>1,3,\*</sup>, Meisong Liao <sup>1</sup>, Juping Ma <sup>1,2</sup>, Xin Wang <sup>1</sup>, Dongbing He <sup>1</sup>, Weiqing Gao <sup>4</sup>,  
Jonathan Knight <sup>5</sup>, Lili Hu <sup>1,3,\*</sup>

<sup>1</sup> Key Laboratory of Materials for High Power Laser, Shanghai Institute of Optics and Fine Mechanics,  
Chinese Academy of Sciences, Shanghai 201800, China

<sup>2</sup> Center of Materials Science and Optoelectronics Engineering, University of Chinese Academy of  
Sciences, Beijing 100049, China

<sup>3</sup> Hangzhou Institute for Advanced Study, University of Chinese Academy of Sciences, Hangzhou 310024,  
China

<sup>4</sup> Department of Optical Engineering, Hefei University of Technology, Hefei 230601, China

<sup>5</sup> Centre for Photonics and Photonic Materials, Department of Physics, University of Bath, Claverton  
Down, Bath, BA2 7AY, United Kingdom

**Abstract:** In this work, we systematically study spectroscopic properties of Tb<sup>3+</sup>/Dy<sup>3+</sup> co-doped phosphate glasses in the visible spectral region and explore the sensitization role of Dy<sup>3+</sup> in the enhancement of visible fluorescence of Tb<sup>3+</sup> ions. Judd–Ofelt parameters  $\Omega_2$  and  $\Omega_4/\Omega_6$  of the phosphate glass as host for Tb<sup>3+</sup> are calculated as  $21.60 \times 10^{-20} \text{ cm}^2$  and 0.73 respectively based on the measured spectral absorption. Multiple energy transfer routes from Dy<sup>3+</sup> to Tb<sup>3+</sup> and their efficiencies are characterized and the enhanced fluorescence properties of Tb<sup>3+</sup> are investigated, including the emission spectral strength and the spontaneous emission lifetime as functions of Dy<sup>3+</sup> doping concentration. The efficient non-radiative energy transfer processes between Dy<sup>3+</sup> and Tb<sup>3+</sup> allow a moderate concentration level of Tb<sup>3+</sup> to achieve favorably stronger spectral absorption at blue and ultraviolet wavelengths but almost negligible up-conversion. Tb<sup>3+</sup>/Dy<sup>3+</sup> co-doped phosphate glass shows promising potential for phosphors and lasing operation at visible wavelengths.

**Keywords:** Dy<sup>3+</sup>/Tb<sup>3+</sup>; phosphate glass; luminescence; energy transfer process

---

\* Corresponding author.

E-mail address: [yufei@siom.ac.cn](mailto:yufei@siom.ac.cn) (F. Yu), [hulili@siom.ac.cn](mailto:hulili@siom.ac.cn) (L. Hu)

## 1. Introduction

In recent years, visible luminescence of  $\text{Tb}^{3+}$  ions doped in crystal, ceramic and glass, has found various applications in display techniques, visible light communication and medical treatment <sup>1-6</sup>. Particularly, lasing operation in the visible spectral region has already been demonstrated in  $\text{Tb}^{3+}$  doped crystals, e.g.  $\text{CaF}_2$  <sup>7</sup>,  $\text{LiLuF}_4$  <sup>7</sup>,  $\text{LiYF}_4$  <sup>8</sup>,  $\text{LaF}_3$  <sup>9</sup>,  $\text{KY}_3\text{F}_{10}$  <sup>9</sup>,  $\text{BaY}_2\text{F}_8$  <sup>9</sup>,  $\text{BaLu}_2\text{F}_4$  <sup>9</sup> as well as in fluoride glass fibers <sup>10-12</sup>.

$\text{Tb}^{3+}$  doped fluoride glass was investigated for visible luminescence since 1989 <sup>13</sup>. Generally, the low-energy phonon density distribution of the fluoride glass mitigates the cross relaxation processes, which is favorable for a high concentration of rare-earth ions, and makes it an attractive material for gain fiber <sup>10-12</sup>. <sup>14</sup>. In 2007,  $\text{Tb}^{3+}$  doped fluoride glass of 1 wt% concentration realized a gain of 5.3 dB at 540 nm wavelength <sup>11</sup>. In 2008, the first continuous-wave laser operation at 542 nm in a fluoride glass fiber was reported where 1.6 mW output power with 8.4 % slope efficiency was measured <sup>12</sup>.

Visible emissions in rare-earth ions doped oxide glasses usually suffer from degradation of emission strength due to the cross relaxation effect <sup>15</sup>. Uniquely,  $\text{Tb}^{3+}$  ions with  $^5\text{D}_4$ -multiplet are regarded as a promising doping candidate which is assumed to be largely absent from cross relaxation processes due to the lack of acceptor levels. The feasibility of doping  $\text{Tb}^{3+}$  ion in phosphate <sup>16</sup>, silicate <sup>17</sup>, and borate <sup>18</sup> glasses has been explored. Unfortunately the weak absorption cross section of  $\text{Tb}^{3+}$  around  $10^{-22} \text{ cm}^2$  in the blue spectral region <sup>9</sup> challenges its practical application.

Among oxide glasses, phosphate glasses are known for high transparency, high solubility of rare-earth ions, low photo-darkening and mature manufacturing technology <sup>19-21</sup>. Although in principle phosphate glasses allow a much higher doping concentration of  $\text{Tb}^{3+}$ , multi-photon absorption <sup>9</sup> counterbalances the benefits of increased dopant concentration in practice. To address the dilemma,  $\text{Dy}^{3+}$  assisted energy transfer (ET) process has been proposed to enhance the visible fluorescence of  $\text{Tb}^{3+}$  under a moderate

concentration level and investigated in hosts of borate <sup>22</sup>, silicate <sup>23</sup> oxyfluorosilicate <sup>24</sup> glasses, which indicated Dy<sup>3+</sup> ion as a good sensitizer for the visible emission of Tb<sup>3+</sup> ions.

In the previous studies of Dy<sup>3+</sup>/Tb<sup>3+</sup> co-doped phosphate glasses 25-27, the potential of using Dy<sup>3+</sup> to sensitize Tb<sup>3+</sup> in phosphate glass for visible lasing application still remained unexplored. In this work, we focus on the spectroscopic properties of Tb<sup>3+</sup> ions in Dy<sup>3+</sup>/Tb<sup>3+</sup> co-doped phosphate glasses, and systematically characterize the dependence of spectral and temporal properties of Tb<sup>3+</sup> emission on pump wavelength and Dy<sup>3+</sup> concentration, which are key to understand the sensitization effect of Dy<sup>3+</sup> ions. Energy transfer routes and corresponding efficiencies between Dy<sup>3+</sup> and Tb<sup>3+</sup> ions are investigated based on experimental measurement of enhanced absorption, excitation and fluorescence spectra of Tb<sup>3+</sup> ions in the Dy<sup>3+</sup>/Tb<sup>3+</sup> co-doped phosphate glass. We experimentally confirm much higher Judd–Ofelt parameters and longer lifetime of Tb<sup>3+</sup> in our phosphate glass, with a promising potential for laser operation at visible wavelengths.

## 2. Glass synthesis and characterization methodology

### 2.1 Glass synthesis

The sample glasses are fabricated by composition (in mol%) of 65P<sub>2</sub>O<sub>5</sub>-15Al<sub>2</sub>O<sub>3</sub>-10K<sub>2</sub>O-(10-x-y)Y<sub>2</sub>O<sub>3</sub>-xTb<sub>2</sub>O<sub>3</sub>-yDy<sub>2</sub>O<sub>3</sub> (x=1, y=0, 0.1, 0.5, 1, 2; x=0, y=1; x=0, 0.5, 1, 2, 4, y=0.5) which are denoted as T1, T1D0.1, T1D0.5, T1D1 and T1D2, respectively), as listed in Table 1. Analytical reagents P<sub>2</sub>O<sub>5</sub>, Al<sub>2</sub>O<sub>3</sub>, K<sub>2</sub>CO<sub>3</sub> and high purity Tb<sub>2</sub>O<sub>3</sub>, Dy<sub>2</sub>O<sub>3</sub> (99.99 wt.% Aladdin Chemical Co.) were used as raw materials. Compounds were well mixed and melted in platinum crucibles at 1150°C for 2 h in the atmosphere, cast onto a preheated steel plate, and then annealed at 450°C for 3 h. The prepared glass samples (15 mm × 15 mm × 1.2 mm each) were double-polished for characterization.

Table 1. Composition of Tb<sup>3+</sup>/Dy<sup>3+</sup> co-doped phosphate glasses.

Glass compositions (mol%)
---------------------------

Samples	P <sub>2</sub> O <sub>5</sub>	Al <sub>2</sub> O <sub>3</sub>	K <sub>2</sub> O	Y <sub>2</sub> O <sub>3</sub>	Tb <sub>2</sub> O <sub>3</sub>	Dy <sub>2</sub> O <sub>3</sub>
T1	65	15	10	9	1	-
T1D0.1	65	15	10	8.9	1	0.1
T1D0.5	65	15	10	8.5	1	0.5
T1D1	65	15	10	8	1	1
T1D2	65	15	10	7	1	2
D1	65	15	10	9	-	1
D0.5	65	15	10	9.5	-	0.5
T0.5D0.5	65	15	10	9	0.5	0.5
T2D0.5	65	15	10	7.5	2	0.5
T4D0.5	65	15	10	5.5	4	0.5

## 2.2 Measurement method

Phases of the samples were characterized by X-ray diffraction (XRD, Rigaku RINT-2000) with Cu K $\alpha$  radiation (0.154 nm). The element distribution of samples was characterized by JXA8230 electron probe microscopy analysis (EPMA). Scanning electron microscopy (SEM) images of samples were acquired on an SU1080 microscopy (Hitachi, Japan). The refractive index was measured by a waveguide prism coupling instrument 1010/M (Metricon Co., USA). The absorption spectra of Dy<sup>3+</sup>/Tb<sup>3+</sup> co-doped phosphate glass samples were measured with a UV/VIS/NIR spectrophotometer (Perkin Elmer Lambda 900) using Xe discharged lamp as light source. The excitation, emission spectra and fluorescence lifetime of samples were obtained by using an Edinburg FL920-type spectrophotometer. All measurements were carried out at room temperature.

## 3. Characterization and discussion

### 3.1 Dopant distribution in samples

The XRD patterns of all Dy<sup>3+</sup>/Tb<sup>3+</sup> co-doped phosphate glasses are shown in Fig. 1, and a broad refraction peak at around  $2\theta = 25^\circ$  was observed in all glass samples. Based on the study on the fundamentals of amorphous solids<sup>28</sup>, the broad refraction peak is ascribed to the immaterial orientation of the amorphous glass with regard to the X-ray beam as there is no any crystalline plane. The diffraction angle  $2\theta$  is related to the region of local random network in glasses (from Bragg's law:  $\lambda = 2d \sin\theta$ ). We pick T1D1 and

characterize 2D elemental distributions of P, O, Al and K shown in Fig. 2a–e, whereas the signals of low-concentrated  $\text{Tb}^{3+}$  and  $\text{Dy}^{3+}$  were too weak to detect. To further examine the dopant uniformity, we use EPMA to scan sample T1D2 and homogeneous distributions of  $\text{Tb}^{3+}$  and  $\text{Dy}^{3+}$  ions in Fig. 2f.

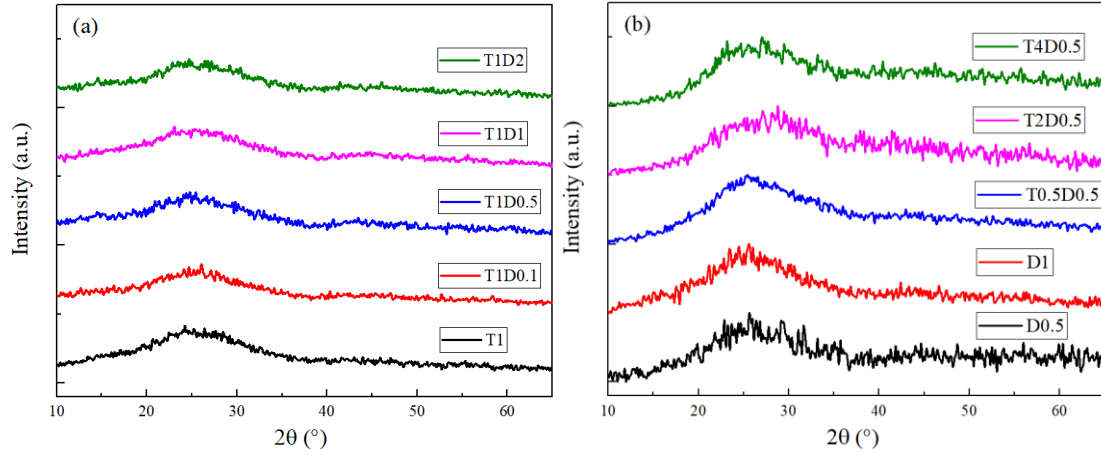


Fig. 1. XRD patterns of  $\text{Tb}^{3+}/\text{Dy}^{3+}$  co-doped phosphate glasses.

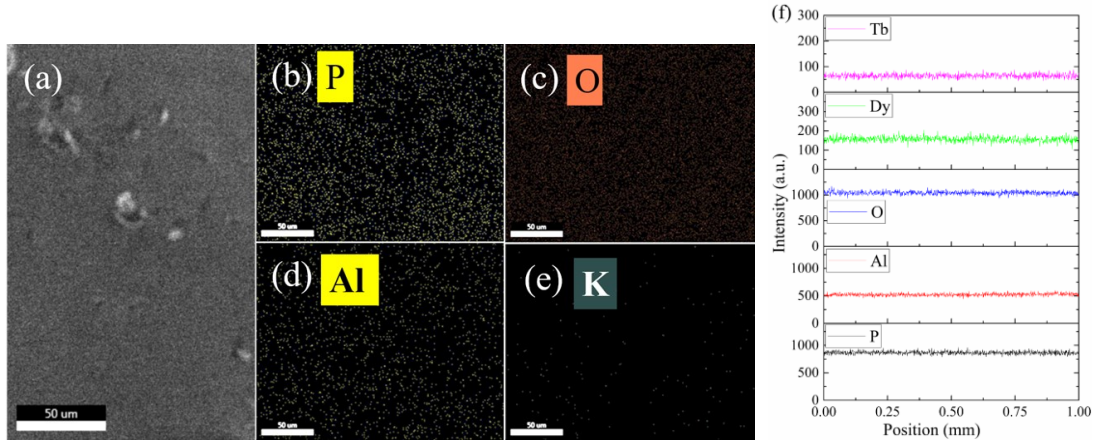


Fig. 2. (a) SEM images of glass surface and two-dimensional elemental distributions of (b) P, (c) O, (d) Al and (e) K in the T1D1 sample, and (f) line scan of P, Al, O, Dy and Tb in sample T1D2.

### 3.2 Absorption measurement and Judd–Ofelt analysis

The measured absorption spectra of all glass samples in the wavelength range from 300 to 2500 nm are shown in Fig. 3a and b. Absorption peaks of  $\text{Tb}^{3+}$  ions in  $\text{Dy}^{3+}$  free sample T1 locate at 338, 350, 359, 366, 377, 485, 1885, 1903 and 2209 nm corresponding to transitions from ground state  $^7\text{F}_6$  to excited states of  $^5\text{L}_7$ ,  $^5\text{L}_9$ ,  $^5\text{G}_5$ ,  $^5\text{L}_{10}$ ,  $^5\text{D}_3$ ,  $^5\text{D}_4$ ,  $^7\text{F}_1$ ,  $^7\text{F}_2$  and  $^7\text{F}_3$ , respectively. Absorption in  $\text{Dy}^{3+}/\text{Tb}^{3+}$  co-doped samples at 350, 364, 377, 386, 425, 452, 472 and 1682 nm is due to transitions of  $\text{Dy}^{3+}$  ions from ground state  $^6\text{H}_{15/2}$  to the  $^4\text{M}_{15/2}$ ,  $^4\text{I}_{11/2}$ ,  $^4\text{I}_{13/2}$ ,  $^4\text{F}_{7/2}$ ,  $^4\text{G}_{11/2}$ ,  $^4\text{I}_{15/2}$ ,  $^4\text{F}_{9/2}$  and  $^6\text{H}_{11/2}$  excited states, as illustrated by the energy level diagrams

<sup>25</sup> in Fig. 3c. In the single dopant samples, Dy<sup>3+</sup> ions present much stronger absorption than Tb<sup>3+</sup> ions at the same concentration level at UV and blue wavelengths. By comparing Fig. 3a and b, Tb<sup>3+</sup> ions show higher absorption at infrared wavelength region, whereas Dy<sup>3+</sup> ions exhibit much stronger absorption at UV and blue wavelengths.

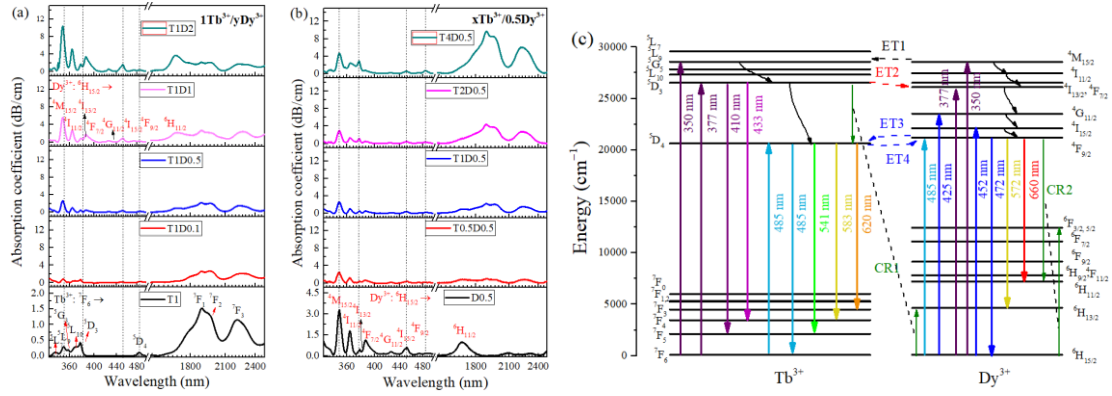


Fig. 3. Measured absorption spectra of (a) 1Tb<sup>3+</sup>/yDy<sup>3+</sup> (y=0, 0.1, 0.5, 1, 2), (b) xTb<sup>3+</sup>/0.5Dy<sup>3+</sup> (x=0, 0.5, 1, 2, 4) in phosphate glasses, and (c) energy level diagrams of Tb<sup>3+</sup> and Dy<sup>3+</sup> ions with possible transfer routes in between <sup>25</sup>.

Table 2 summarizes absorption cross-sections ( $\sigma_a$ ) of Dy<sup>3+</sup> and Tb<sup>3+</sup> ions at different wavelengths calculated by  $\sigma_a = 2.303OD(\lambda)/NI$ , in which  $OD(\lambda)$  is optical density obtained from the spectrophotometer,  $l$  the thickness of samples,  $N$  the concentration ( $N = \rho m_w N_A / M_w$ ,  $\rho$  is density of sample,  $m_w$  weight concentration of dopant ions,  $N_A = 6.022 \times 10^{23} \text{ mol}^{-1}$  Avogadro number,  $M_w$  molar mass). Dy<sup>3+</sup> ions present a stronger absorption at 350 nm by an order of magnitude than that of Tb<sup>3+</sup> ions in phosphate glasses. Four possible energy transfer routes <sup>23, 25</sup>, ET1 (Dy<sup>3+</sup>: <sup>4</sup>M<sub>15/2</sub> + Tb<sup>3+</sup>: <sup>7</sup>F<sub>6</sub> → Dy<sup>3+</sup>: <sup>6</sup>H<sub>15/2</sub> + Tb<sup>3+</sup>: <sup>5</sup>L<sub>9</sub>), ET2 (Tb<sup>3+</sup>: <sup>5</sup>D<sub>3</sub> + Dy<sup>3+</sup>: <sup>6</sup>H<sub>15/2</sub> → Tb<sup>3+</sup>: <sup>7</sup>F<sub>6</sub> + Dy<sup>3+</sup>: <sup>4</sup>F<sub>7/2</sub> + phonon), ET3 and 4 (Dy<sup>3+</sup>: <sup>4</sup>F<sub>9/2</sub> + Tb<sup>3+</sup>: <sup>7</sup>F<sub>6</sub> ↔ Dy<sup>3+</sup>: <sup>6</sup>H<sub>15/2</sub> + Tb<sup>3+</sup>: <sup>5</sup>D<sub>4</sub> + phonon) shown in Fig. 3c, makes it possible to sensitize Tb<sup>3+</sup> ions in phosphate glass for visible emission by Dy<sup>3+</sup> ions co-doping.

Table 2. Absorption cross-sections  $\sigma_a$  of Tb<sup>3+</sup> and Dy<sup>3+</sup> ions at UV and visible wavelengths

Transitions	Wavelength (nm)	$\sigma_a (\times 10^{-22} \text{ cm}^2)$ of Tb <sup>3+</sup>	$\sigma_a (\times 10^{-22} \text{ cm}^2)$ of Dy <sup>3+</sup>
Tb <sup>3+</sup> : <sup>7</sup> F <sub>6</sub> → <sup>5</sup> L <sub>9</sub>	350	2.9	
Tb <sup>3+</sup> : <sup>7</sup> F <sub>6</sub> → <sup>5</sup> D <sub>3</sub>	377	4.3	

Tb <sup>3+</sup> : <sup>7</sup> F <sub>6</sub> → <sup>5</sup> D <sub>4</sub>	485	1.1	
Dy <sup>3+</sup> : <sup>6</sup> H <sub>15/2</sub> → <sup>4</sup> M <sub>15/2</sub>	350		62.8
Dy <sup>3+</sup> : <sup>6</sup> H <sub>15/2</sub> → <sup>4</sup> I <sub>11/2</sub>	364		35.1
Dy <sup>3+</sup> : <sup>6</sup> H <sub>15/2</sub> → <sup>4</sup> I <sub>13/2</sub>	377		9.6
Dy <sup>3+</sup> : <sup>6</sup> H <sub>15/2</sub> → <sup>4</sup> I <sub>15/2</sub>	452		8.9
Dy <sup>3+</sup> : <sup>6</sup> H <sub>15/2</sub> → <sup>4</sup> F <sub>9/2</sub>	485		2.3

Based on Judd–Ofelt (J–O) theory<sup>29, 30</sup>, the experimental strength ( $f_{\text{exp}}$ ) of transitions can be calculated

from absorption spectra by the following equation:

$$f_{\text{exp}} = \frac{2.303mc^2}{\pi Nle^2 \bar{\lambda}^2} \int \log_{10} \left( \frac{I(\lambda)}{I_0} \right) d\lambda \quad (1)$$

where  $m$  is the electron mass,  $e$  the charge,  $c$  the velocity of light in vacuum, and  $\bar{\lambda}$  the mean wavelength of the transition photon. The theoretical oscillator strength ( $f_{\text{cal}}$ ) of radiative  $4f \rightarrow 4f$  transitions from an initial  $J$  to a final  $J'$  states can be calculated:

$$f_{\text{cal}}(J; J') = \frac{8\pi^2 mc}{3h(2J+1)\bar{\lambda}} \left[ \frac{(n^2+2)^2}{9n} S_{\text{ed}}(J; J') + n S_{\text{md}}(J; J') \right] \quad (2)$$

$$S_{\text{ed}}(J; J') = \sum_{t=2,4,6} \Omega_t \left| \left\langle (S, L)J \left\| U^t \right\| (S', L')J' \right\rangle \right|^2 \quad (3)$$

$$S_{\text{md}}(J, J') = \left( \frac{h}{4\pi mc} \right)^2 \sum_{t=2,4,6} \left| \left\langle (S, L)J \left\| \bar{L} + 2\bar{S} \right\| (S', L')J' \right\rangle \right|^2 \quad (4)$$

where  $n$  is the refractive index of the host, the terms  $\left| \left\langle (S, L)J \left\| U^t \right\| (S', L')J' \right\rangle \right|^2$  are the double-reduced matrix elements of unit tensor operators that are considered to be independent of host materials and its values of Tb<sup>3+</sup> ions are given by Carnall et al.<sup>31</sup>, and  $\Omega_t$  ( $t=2, 4, 6$ ) are the J–O parameters that can be calculated by a least-square fitting approach. Table 3 shows good agreement between  $f_{\text{exp}}$  and  $f_{\text{cal}}$ . The root-mean-square deviation ( $\delta_{\text{rms}}$ ) is  $\pm 0.12 \times 10^{-6}$  implying a good quality of fitting. It is noted that J–O parameters of Tb<sup>3+</sup> ions in T1 sample are calculated from the absorption bands of <sup>7</sup>F<sub>6</sub> → <sup>5</sup>D<sub>4</sub> and <sup>7</sup>F<sub>1,2,3</sub> (shown in Fig. 3a) rather than the absorption in the blue region (300–400 nm) where the absorption features are too complex to calculate<sup>32, 33</sup>.



Table 3. Peak wavelength of absorption bands of  $\text{Tb}^{3+}$  ions in T1 sample as well as the experimental  $f_{\text{exp}}$  and calculated  $f_{\text{cal}}$  oscillator strengths.

Transition	$\lambda_{\text{peak}}$ (nm)	$f_{\text{exp}} (\times 10^{-6})$	$f_{\text{cal}} (\times 10^{-6})$
${}^7\text{F}_6 \rightarrow {}^5\text{D}_4$	484	0.060	0.060
${}^7\text{F}_6 \rightarrow {}^7\text{F}_1$	1895	0.585	0.495
${}^7\text{F}_6 \rightarrow {}^7\text{F}_2$	1903	0.540	0.620
${}^7\text{F}_6 \rightarrow {}^7\text{F}_3$	2209	0.645	0.629
$\delta_{\text{rms}} = \pm 0.12 \times 10^{-6}$			

Table 4 compares the J–O parameters of  $\text{Tb}^{3+}$  in our T1 sample with other reported host materials<sup>18, 32–35</sup>. The parameter  $\Omega_2$  reflects directly the asymmetry of local environment around  $\text{Tb}^{3+}$  ions and the covalence degree between  $\text{Tb}^{3+}$  and ligand ions. The spectroscopic quality factor  $\Omega_4/\Omega_6$  is important for evaluating the stimulated emission behavior<sup>34</sup>. A higher values of  $\Omega_2$  parameter ( $21.60 \times 10^{-20} \text{ cm}^2$ ) and  $\Omega_4/\Omega_6$  ratio of 0.73 for  $\text{Tb}^{3+}$  ions are obtained in our phosphate glass (T1 sample) than those reported in previous studies, implying that a stronger local electric field results in a higher degree of asymmetry around the rare-earth ions and gives rise to a more efficient stimulated emission of  $\text{Tb}^{3+}$  ions in our phosphate glass.

Table 4. Comparison of Judd–Ofelt parameters of  $\text{Tb}^{3+}$  ions in different host materials.

Host materials	$\Omega_2 (10^{-20} \text{ cm}^2)$	$\Omega_4 (10^{-20} \text{ cm}^2)$	$\Omega_6 (10^{-20} \text{ cm}^2)$	$\Omega_4/\Omega_6$	Reference
Lead borate glass	13.23	1.23	2.96	0.42	32
Lead telluroborate glass	11.98	2.87	10.51	0.27	33
Zinc borophosphate glass	11.26	1.02	3.00	0.34	34
Borate glass	6.95	1.28	2.91	0.44	18
Fluoride glass	13.40	2.15	4.90	0.44	35
Phosphate glass (T1)	21.60	1.56	2.15	0.73	Our work

### 3.3 Excitation and luminescence measurement

Figure 4 compares the measured excitation spectra of the T1 and T1D0.5 samples by monitoring the emission at 541 nm, as well as D1 sample monitored at 572 nm. According to Fig. 4, we select 350, 377 and 485 nm as pumping wavelengths, corresponding to  $\text{Tb}^{3+}$ :  ${}^7\text{F}_6 \rightarrow {}^5\text{L}_9$  +  $\text{Dy}^{3+}$ :  ${}^6\text{H}_{15/2} \rightarrow {}^4\text{M}_{15/2}$ ,  $\text{Tb}^{3+}$ :  ${}^7\text{F}_6 \rightarrow {}^5\text{D}_3$  +  $\text{Dy}^{3+}$ :  ${}^6\text{H}_{15/2} \rightarrow {}^4\text{F}_{7/2}$  and  $\text{Tb}^{3+}$ :  ${}^7\text{F}_6 \rightarrow {}^5\text{D}_4$  +  $\text{Dy}^{3+}$ :  ${}^6\text{H}_{15/2} \rightarrow {}^4\text{F}_{9/2}$ , respectively, and investigate the fluorescence of  $\text{Tb}^{3+}$  ions as a function of  $\text{Dy}^{3+}$  concentration. The corresponding emission spectra are shown in Fig. 5.

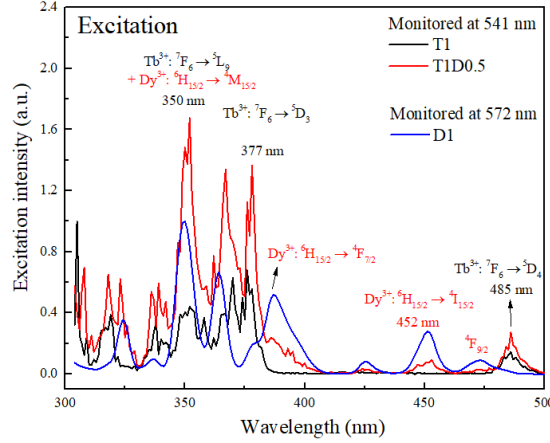


Fig. 4. Excitation spectra of the samples T1 and T1D0.5 by monitoring emission at 541 nm as well as D1 sample monitored at 572 nm.

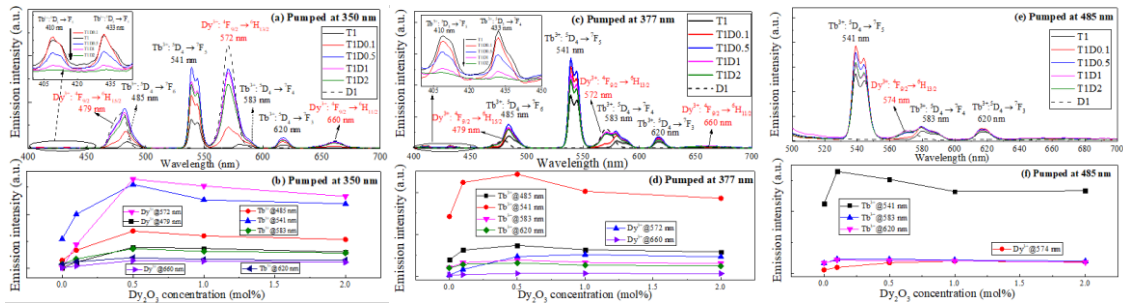


Fig. 5. Emission spectra of 1Tb<sup>3+</sup>/yDy<sup>3+</sup> (y=0, 0.1, 0.5, 1, 2) co-doped phosphate glasses pumped by (a) 350 nm, (c) 377 nm and (e) 485 nm, and the corresponding trends of main emission intensities as a function of Dy<sup>3+</sup> concentration pumped by (b) 350 nm, (d) 377 nm and (f) 485 nm, respectively.

In Fig. 5a, the emission of Tb<sup>3+</sup> ions peaked at 541 nm is observed in T1 and much enhanced after introducing Dy<sup>3+</sup> ions. By pumping at 350 nm wavelength, Tb<sup>3+</sup> ions have a rapid thermal relaxation that would populate <sup>5</sup>D<sub>3</sub> from <sup>5</sup>L<sub>9</sub><sup>25</sup>, and subsequently radiate to <sup>7</sup>F<sub>5</sub> and <sup>7</sup>F<sub>4</sub> states, giving rise to emission peaked at 412 and 435 nm, respectively (as shown in Fig. 3c). Meanwhile, electrons in <sup>5</sup>D<sub>3</sub> state of Tb<sup>3+</sup> would non-radiatively quench to <sup>5</sup>D<sub>4</sub> state by multi-phonon relaxation or cross relaxation (CR) processes, and then radiate to <sup>7</sup>F<sub>6</sub>, <sup>7</sup>F<sub>5</sub>, <sup>7</sup>F<sub>4</sub> and <sup>7</sup>F<sub>3</sub> states corresponding to the emissions peaked at 485, 541, 583 and 620 nm, respectively. Under pumping at 350 nm, Dy<sup>3+</sup> ions are excited to <sup>4</sup>M<sub>15/2</sub> state and found quickly quenched to <sup>4</sup>F<sub>9/2</sub> state by thermal relaxation, and then radiate to <sup>6</sup>H<sub>15/2</sub>, <sup>6</sup>H<sub>13/2</sub> and <sup>6</sup>H<sub>11/2</sub> states which give rise to emissions at 479, 572 and 660 nm respectively. The introduction of Dy<sup>3+</sup> ions helps population of Tb<sup>3+</sup>: <sup>5</sup>D<sub>3</sub> state through the ET1 process (shown in Fig. 3c) efficiently. From the enhanced emission at 485, 541 and

620 nm wavelengths (derived from  $\text{Tb}^{3+}$ :  $^5\text{D}_4$  state shown in Fig. 5a), we confirm a more efficient energy transfer process ET3 (shown in Fig. 3c) from  $\text{Dy}^{3+}$  ions to populate the  $\text{Tb}^{3+}$ :  $^5\text{D}_4$  state. It is noted that the ET2 and CR1 ( $\text{Tb}^{3+}$ :  $^5\text{D}_3 + \text{Dy}^{3+}$ :  $^6\text{H}_{15/2} \rightarrow \text{Tb}^{3+}$ :  $^5\text{D}_4 + \text{Dy}^{3+}$ :  $^6\text{H}_{13/2} + \text{phonon}$ , shown in Fig. 3c) processes can reduce the emission strengths at 410 and 433 nm wavelengths, when  $\text{Dy}_2\text{O}_3$  doping concentration is more than 0.5 mol%.

The emissions strength of  $\text{Tb}^{3+}$  reaches the maximum in all samples when introducing  $\text{Dy}^{3+}$  at 0.5 mol%  $\text{Dy}_2\text{O}_3$  concentration. As the doping concentration of  $\text{Dy}^{3+}$  rises further, emission intensities of both  $\text{Dy}^{3+}$  and  $\text{Tb}^{3+}$  ions in T1D1 and 2 samples are declined and maintained, and we ascribe it to the counterbalance out of concentration quenching effect<sup>36</sup>, in which the ET4 process from  $\text{Tb}^{3+}$  to  $\text{Dy}^{3+}$  ions, and possible CR2 ( $\text{Dy}^{3+}$ :  $^4\text{F}_{9/2} + ^6\text{H}_{15/2} \rightarrow ^6\text{H}_{11/2} + ^6\text{F}_{3/2}$  shown in Fig. 3c) occurred between  $\text{Dy}^{3+}$  ions<sup>37</sup>, resulted in the inefficient emission behaviors of  $\text{Tb}^{3+}$  and  $\text{Dy}^{3+}$  ions respectively.

Similar to 350 nm pumping wavelength, 377 nm pump will excite  $\text{Tb}^{3+}$ :  $^5\text{D}_3$  state, radiating to  $^7\text{F}_5$  (412 nm) and  $^7\text{F}_4$  (435 nm) states, meanwhile the ET2, ET3 and CR1 processes populate the  $\text{Tb}^{3+}$ :  $^5\text{D}_4$  state, radiating to  $^7\text{F}_6$  (485 nm),  $^7\text{F}_5$  (541 nm),  $^7\text{F}_4$  (583 nm) and  $^7\text{F}_3$  (620 nm) states. Emissions peaked at 485, 541, 583 and 620 nm show almost the same trends as that by pumping at 350 nm. For  $\text{Dy}^{3+}$  ions, a thermal relaxation will populate  $^4\text{F}_{9/2}$  from  $^4\text{F}_{7/2}$  (377 nm) states as shown in Fig. 3c, and generate 479, 572 and 660 nm emissions. The weak emissions of  $\text{Dy}^{3+}$  ions can be attributed to its lower absorption at 377 nm as shown in Table 1 and Fig. 4.

In Fig. 5e, the main emission at 541 nm is generated by pumping  $\text{Tb}^{3+}/\text{Dy}^{3+}$  co-doped phosphate glasses with 485 nm. The  $\text{Tb}^{3+}$ :  $^5\text{D}_4$  state is populated by 485 nm pump and ET3 process from  $\text{Dy}^{3+}$  ions, radiating to  $^7\text{F}_6$  (485 nm),  $^7\text{F}_5$  (541 nm),  $^7\text{F}_4$  (583 nm) and  $^7\text{F}_3$  (620 nm) states. The maximum emission of  $\text{Tb}^{3+}$  appears in the T1D0.1 sample and the concentration quenching effect takes place for  $\text{Dy}_2\text{O}_3$  concentration more

than 0.5 mol%, which are attributed to the lower absorption cross-sections of both  $\text{Tb}^{3+}$  and  $\text{Dy}^{3+}$  ions at 485 nm. It can be concluded for  $\text{Dy}^{3+}$  ions that all the pumping wavelengths (350, 377 and 485 nm) populate the  $\text{Dy}^{3+}: {}^4\text{F}_{9/2}$  state, and generate emissions peaked at 479, 572 and 660 nm. Besides, 350 nm is the most efficient pump wavelength for both the 541 nm emission of  $\text{Tb}^{3+}$  and 572 nm emission of  $\text{Dy}^{3+}$  ions in  $\text{Tb}^{3+}/\text{Dy}^{3+}$  co-doped phosphate glasses.

### 3.4 Fluorescence lifetimes of $\text{Tb}^{3+}$ ion

The fluorescence decay curve of  $\text{Tb}^{3+}: {}^5\text{D}_4 \rightarrow {}^7\text{F}_5$  transition emitting at around 541 nm are measured as a function of  $\text{Dy}^{3+}$  concentrations under excitations of 350, 485 and 452 nm respectively, shown in Fig. 6. Using a logarithmic scale for the axis of emission intensity we confirm an almost linear fluorescence decay as function of time, indicating an exponential decay behavior. As shown in Fig. 6d, the longest lifetime of  $\text{Tb}^{3+}: {}^5\text{D}_4$  state is found in T1D0.1 with 0.1 mol%  $\text{Dy}_2\text{O}_3$  concentration for all pump wavelengths, which we ascribed to the ET3 process, whereas the slightly decreased lifetime<sup>38</sup> is attributed to the ET4 and CR2 processes shown in Fig. 3c. The trends of lifetime of  $\text{Tb}^{3+}: {}^5\text{D}_4$  level as function of  $\text{Dy}^{3+}$  concentration almost show no dependence on pumping wavelengths as illustrated in Fig. 6d.

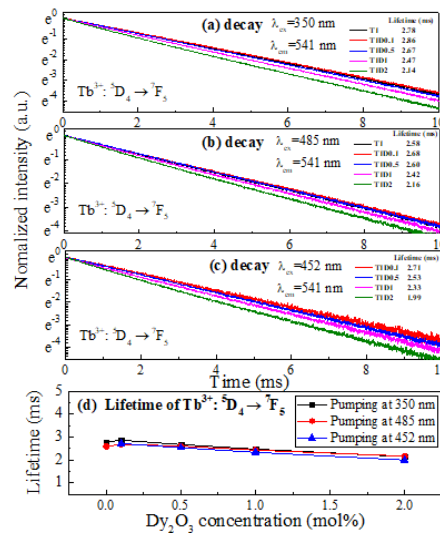


Fig. 6. Decay curves of transition  $\text{Tb}^{3+}: {}^5\text{D}_4 \rightarrow {}^7\text{F}_5$  pumped at (a) 350 nm, (b) 485 nm and (c) 452 nm, and (d) the calculated lifetime as a function of  $\text{Dy}^{3+}$  concentration.

Table 5. Measured lifetime of the  $\text{Tb}^{3+}: {}^5\text{D}_4 \rightarrow {}^7\text{F}_5$  transition in our work (pumped by 350 nm) and

reported literatures.

Host	Tb <sub>2</sub> O <sub>3</sub> concentration (mol%)	Lifetime (ms)	Reference
Lead borate glass	1.0	1.76	32
Lead telluroborate glass	1.0	0.83	33
Zinc borophosphate glass	0.9	1.89	34
Fluoride glass	0.5	1.21	35
T1	1.0	2.78	Our work
T1D0.1	1.0	2.86	Our work
T1D0.5	1.0	2.67	Our work
T1D1	1.0	2.47	Our work
T1D2	1.0	2.14	Our work

Table 5 compares the measured lifetime of Tb<sup>3+</sup>: <sup>5</sup>D<sub>4</sub>→<sup>7</sup>F<sub>5</sub> transition in various host materials <sup>32-35</sup>. The

longest 2.86 ms lifetime of Tb<sup>3+</sup>: <sup>5</sup>D<sub>4</sub> is measured in T1D0.1 sample.

### 3.5 Energy transfer efficiency and mechanism

The results of Fig. 4–6 show how the concentration of Dy<sup>3+</sup> ions affect the visible emission properties and fluorescence lifetime of Tb<sup>3+</sup> under the excitation of different pumping wavelength. To further investigate the energy transfer efficiency from Dy<sup>3+</sup> to Tb<sup>3+</sup> ions, we focus on the emission and fluorescence lifetime of xTb<sup>3+</sup>/0.5Dy<sup>3+</sup> (x=0, 0.5, 1, 2, 4) co-doped glass samples by pumping at 425 nm where Tb<sup>3+</sup> presents no absorption.

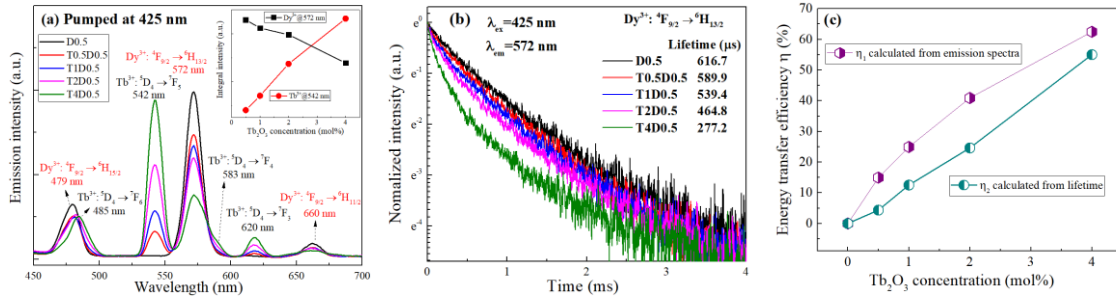


Fig. 7. (a) Emission spectra of xTb<sup>3+</sup>/0.5Dy<sup>3+</sup> (x=0, 0.5, 1, 2, 4) co-doped phosphate glasses pumped by 425 nm, and the inset is the trends of main emission intensities, and (b) the decay curves of transition <sup>4</sup>F<sub>9/2</sub>→<sup>6</sup>H<sub>13/2</sub> of Dy<sup>3+</sup> pumped by 425 nm, inset shows the energy transfer efficiency from Dy<sup>3+</sup> to Tb<sup>3+</sup> ions as a function of Tb<sup>3+</sup> concentration.

Under excitation, Dy<sup>3+</sup>: <sup>4</sup>G<sub>11/2</sub> state is populated and quickly relaxed by transferring energy to <sup>4</sup>F<sub>9/2</sub> state, and radiate to <sup>6</sup>H<sub>15/2</sub> (479 nm), <sup>6</sup>H<sub>13/2</sub> (572 nm) and <sup>6</sup>H<sub>13/2</sub> (660 nm) states as shown in Fig. 3c and Fig. 7a.

Through ET3 process, Tb<sup>3+</sup>: <sup>5</sup>D<sub>4</sub> state is excited with fluorescence emissions peaked at 541, 583 and 620

nm shown in Fig. 7a. After introducing Tb<sup>3+</sup> ions, the energy transfer process ET3 populates the Tb<sup>3+</sup>: <sup>5</sup>D<sub>4</sub> state and gives rise to an increased emissions strength of Tb<sup>3+</sup> at all wavelengths when Tb<sup>3+</sup> concentration rises. Based on the emission spectra, the energy transfer efficiency from Dy<sup>3+</sup> to Tb<sup>3+</sup> ions is defined by  $\eta_1 = 1 - I_{Dy}/(I_{Dy} + I_{Tb})$ <sup>39</sup>, where  $I_{Dy}$  and  $I_{Tb}$  are the integrated intensities of Dy<sup>3+</sup> and Tb<sup>3+</sup> ions, respectively, and the calculated results are plotted in Fig. 7c. We obtained the increasing energy transfer efficiency from Dy<sup>3+</sup> to Tb<sup>3+</sup> ions as a function of Tb<sup>3+</sup> concentration in our phosphate glasses, which are 15.0 %, 24.9 %, 40.9 % and 62.5 % for the T0.5D0.5, T1D0.5, T2D0.5 and T4D0.5 samples, respectively.

To complete our measurement, the decay curves of the transition Dy<sup>3+</sup>: <sup>4</sup>F<sub>9/2</sub> → <sup>6</sup>H<sub>13/2</sub> (572 nm) under excitation at 425 nm are measured as a function of Tb<sup>3+</sup> ions concentration shown in Fig. 7b. A non-exponential decay behavior of Dy<sup>3+</sup> after introducing Tb<sup>3+</sup> ions, especially in the T4D0.5 sample, which confirms the energy transfer processes between Dy<sup>3+</sup> and Tb<sup>3+</sup> ions. The average lifetimes are calculated by

25

$$\tau = \frac{\int_0^{\infty} tI(t)dt}{\int_0^{\infty} I(t)dt} \quad (5)$$

where  $I(t)$  is the emission intensity as function of time  $t$ . The lifetime of Dy<sup>3+</sup> declined from 616.7 μs (D0.5 sample) to 277.2 μs (T4D0.5 sample) as listed in Table 6. Based on the fluorescence lifetime of Dy<sup>3+</sup>, the energy transfer efficiency from Dy<sup>3+</sup> to Tb<sup>3+</sup> ions can be also calculated by <sup>25, 40, 41</sup>  $\eta_2 = 1 - \tau/\tau_0$ , in which  $\tau_0$  and  $\tau$  represent lifetime of donor in the absence and presence of acceptor, respectively) and the calculated results are plotted in Fig. 7c, which are 4.4 %, 12.5 %, 24.6 % and 55.0 % as a function of Tb<sup>3+</sup> concentration for the T0.5D0.5, T1D0.5, T2D0.5 and T4D0.5 samples, respectively. Both  $\eta_1$  and  $\eta_2$  values show a similar increasing trend as function of Tb<sup>3+</sup> ions and the results in our phosphate glasses are on the same level as those found in other host materials <sup>25, 40</sup>, indicating an efficient sensitizer of Dy<sup>3+</sup> ion for the visible emission

of Tb<sup>3+</sup> ions in our phosphate glasses.

Based on Dexter's energy transfer expressions of multipolar interactions<sup>42</sup> and Reisfeld's approximation<sup>43</sup>, the donor-acceptor energy transfer probability ( $P_{DA}$ ) is defined as  $P_{DA} = (1/\tau_d)(\eta_0/\eta - 1)$ , in which  $\tau_d$  is lifetime of donor,  $\eta_0$  and  $\eta$  are the luminescence quantum efficiencies of donor in the absence and presence of acceptor. The  $\eta_0/\eta$  can be approximately calculated by<sup>25, 41, 43</sup>

$$\frac{\eta_0}{\eta} \approx \frac{I_0}{I} \propto C^{\frac{n}{3}} \quad (6)$$

where  $I_0$  and  $I$  are the emission intensities of Dy<sup>3+</sup> (572 nm) in the absence and presence of Tb<sup>3+</sup> ions, respectively,  $C$  is the total concentration of Dy<sup>3+</sup> and Tb<sup>3+</sup> ions, and  $n = 6, 8$  and  $10$  responding to electric dipole-dipole, dipole-quadrupole and quadrupole-quadrupole interactions, respectively. By linear fitting the dependence of  $I_0/I$  on  $C^{n/3}$  as shown in Fig. 8, we obtained a linear relationship with the optimum  $R^2 = 99.98\%$  only when  $n=6$ , which indicates a dominant electric dipole-dipole interaction mechanism responsible for the energy transfer from Dy<sup>3+</sup> to Tb<sup>3+</sup> ions in our phosphate glasses. Table 6 summarized the calculated results discussed above, and in conclusion we obtained an increasing  $\eta_T$  and  $P_{DA}$  from Dy<sup>3+</sup> to Tb<sup>3+</sup> ions as a function of Tb<sup>3+</sup> concentration under excitation at 425 nm. The chromaticity coordinate of emissions in xTb<sup>3+</sup>/0.5Dy<sup>3+</sup> ( $x=0, 0.5, 1, 2, 4$ ) co-doped samples excited at 425 nm in CIE1931 diagram (Fig. 9a) present a yellow-to-green light shift when Tb<sup>3+</sup> concentration rises, indicating a potential application of using our glasses for color adjustable phosphors. Furthermore, we irradiate our Tb<sup>3+</sup>/Dy<sup>3+</sup> co-doped phosphate glass by using a 450 nm multi-mode laser diode (pumping Dy<sup>3+</sup>) as shown in Fig. 9b, and obtained a total reflection of green light in the glass, demonstrating a promising potential of using our Tb<sup>3+</sup>/Dy<sup>3+</sup> co-doped phosphate glass for lasing operation at visible wavelengths.

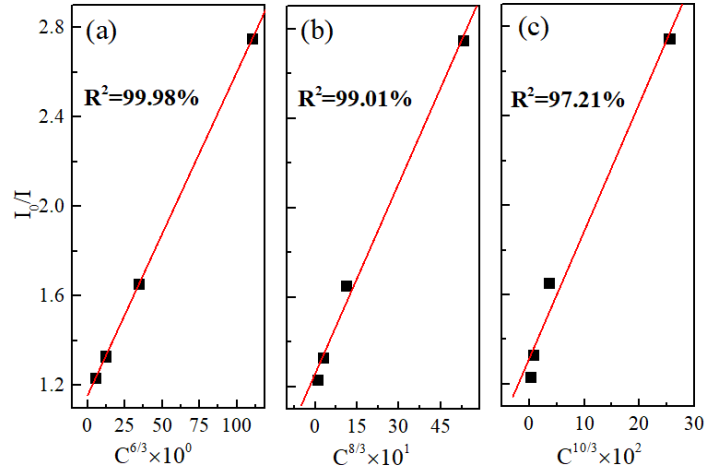


Fig. 8. Dependence of  $I_0/I$  on (a)  $C^{6/3}$ , (b)  $C^{8/3}$  and (c)  $C^{10/3}$ .

Table 6. Measured lifetime  $\tau$  of the  $\text{Dy}^{3+}: {}^4\text{F}_{9/2} \rightarrow {}^6\text{H}_{13/2}$  transition, energy transfer efficiencies  $\eta_T$  and probabilities ( $P_{\text{DA}}$ ) as a function of  $\text{Tb}^{3+}$  concentration under excitation at 425 nm.

Samples	$\tau$ ( $\mu\text{s}$ )	$\eta_T$ (%)	$I_0/I$	$P_{\text{DA}}$ ( $\text{s}^{-1}$ )
D0.5	616.7			
T0.5D0.5	589.9	4.4	1.23	580.9
T1D0.5	539.4	12.5	1.33	874.1
T2D0.5	464.8	24.6	1.65	1405.2
T4D0.5	277.2	55.0	2.75	5795.3

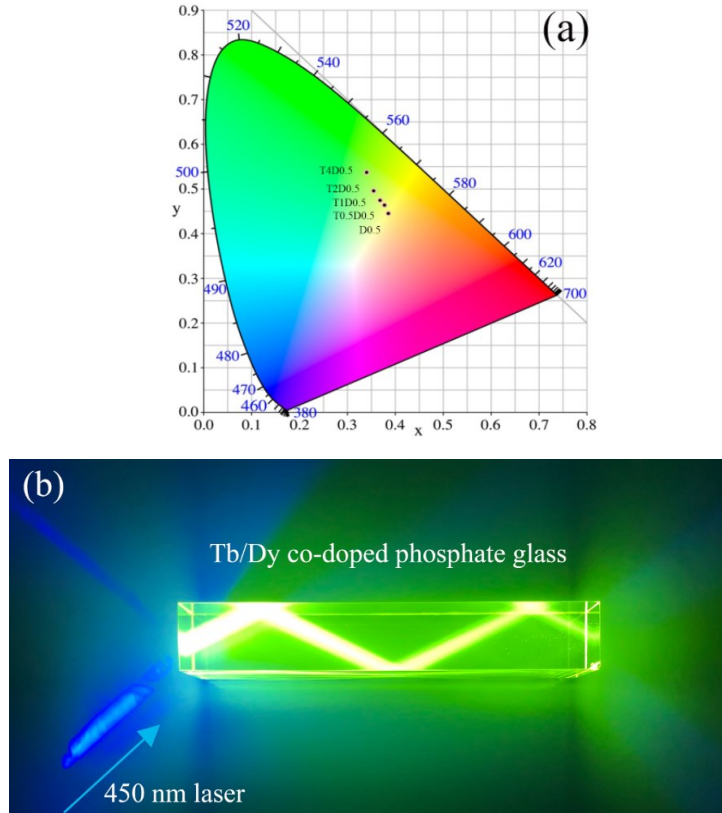


Fig. 9. (a) Chromaticity coordinates of emissions of  $x\text{Tb}^{3+}/0.5\text{Dy}^{3+}$  ( $x=0, 0.5, 1, 2, 4$ ) co-doped samples



excited at 425 nm in CIE1931 diagram (b) photograph of Tb<sup>3+</sup>/Dy<sup>3+</sup> co-doped phosphate glass under irradiation of 450 nm laser diode.

#### 4. Conclusions

In this paper, we study the role of sensitization of Dy<sup>3+</sup> ions played in the enhanced visible emission of Tb<sup>3+</sup> ions in phosphate glasses at various pump wavelengths. We confirm that in the host of phosphate glass, the Judd–Ofelt parameters  $\Omega_2$  and  $\Omega_4/\Omega_6$  for Tb<sup>3+</sup> ions could reach up to  $21.60 \times 10^{-20} \text{ cm}^2$  and 0.73 respectively, highest among all glass hosts as far as we learn. The visible emission (peaked at 485 and 541 nm) of Tb<sup>3+</sup> ions can be much enhanced by the sensitization effect of Dy<sup>3+</sup> under the excitation of 350 and 377 nm with an optimum Dy<sup>3+</sup>/Tb<sup>3+</sup> ions concentration ratio of 0.5:1. The maximum lifetime of Tb<sup>3+</sup>: <sup>5</sup>D<sub>4</sub> (2.86 ms) is measured for the concentration of Dy<sub>2</sub>O<sub>3</sub> around 0.1 mol%. The energy transfer efficiency  $\eta_T$  from Dy<sup>3+</sup> to Tb<sup>3+</sup> is demonstrate an electric dipole-dipole interaction between them and also found a maximum  $\eta_T$  of 55.0% for 4:0.5 ratio of Tb<sup>3+</sup>/Dy<sup>3+</sup> at 425 nm wavelength for pumping. Our studies demonstrate a promising potential of Dy<sup>3+</sup>/Tb<sup>3+</sup> co-doped phosphate glasses for highly efficient visible phosphors and lasing applications.

#### Acknowledgements

This work was supported by National Key R&D Program of China (2018YFB0504500); Key Program for International S&T Cooperation Projects of China (2018YFE0115600); National Natural Science Foundation of China (NSFC, 51972317, 61875052, 61705244 and 61307056); National Natural Science Foundation, International (Regional) Cooperation and Exchange Program (61961136003). Natural Science Foundation of Shanghai (17ZR1433900, 17ZR1434200 and 18ZR1444400). Yu acknowledges the support of Chinese Academy of Sciences (CAS) Pioneer Hundred Talents Program. Knight acknowledges support of Chinese Academy of Sciences Presidential International Fellowship Initiative Grant No. 2019DT0015.

## References

1. Nakanishi J, Yamada T, Fujimoto Y, Ishii O, Yamazaki M. High-power red laser oscillation of 311.4 mW in Pr<sup>3+</sup>-doped waterproof fluoro-aluminate glass fibre excited by GaN laser diode, *Electron Lett.* 2010; 46(46): 1285–1286
2. Park H-A, Lee YK, Im WB, Heo J, Chung WJ. Phosphor in glass with Eu<sup>3+</sup> and Pr<sup>3+</sup>-doped silicate glasses for LED color conversion, *Opt Mater.* 2015; 41: 67–70
3. Jiang S, Guo C, Che K, Luo Z, Du T, Fu H, et al. Visible Raman and Brillouin lasers from a microresonator/ZBLAN-fiber hybrid system, *Photonics Res.* 2019; 7(5): 566–572
4. Zhan L, Cai W, Li N, Lu J, Cai Z, Luo Z, et al. Direct generation of an ultrafast vortex beam in a CVD-graphene-based passively mode-locked Pr:LiYF<sub>4</sub> visible laser, *Photonics Res.* 2019; 7(11): 1209–1213
5. Lam EW, Little TDC. Visible light positioning: moving from 2D planes to 3D spaces [Invited], *Chin Opt Lett.* 2019; 17(3): 030604
6. Fangchen H, Yingjun Z, Nan C, Junlin L, Jianyang S, Fengyi J, et al. Common-anode LED on a Si substrate for beyond 15 Gbit/s underwater visible light communication, *Photonics Res.* 2019; 7(9): 09001019
7. Metz PW, Marzahl D-T, Huber G, Kränkel C. Performance and wavelength tuning of green emitting terbium lasers, *Opt Exp.* 2017; 25(5): 5716–5724
8. Jensen HP, Castleberry D, Gabbe D, Linz A. Stimulated emission at 5445 Å in Tb<sup>3+</sup>: YLF, *IEEE J Quantum Elect.* 1973; 9: 665–665
9. Metz PW, Marzahl D-T, Majid A, Kränkel C, Huber G. Efficient continuous wave laser operation of Tb<sup>3+</sup>-doped fluoride crystals in the green and yellow spectral regions, *Laser Photonics Rev.* 2016; 10(2): 335–344
10. Yamashita T, Ohishi Y. Amplification and lasing characteristics of Tb<sup>3+</sup>-doped fluoride fiber in the 0.54 μm band, *Jpn J Appl Phys.* 2007; 46(No. 41): L991–L993
11. Yamashita T, Ohishi Y. Optical amplification at 0.54 μm by Tb<sup>3+</sup>-doped fluoride fibre, *Electron Lett.* 2007; 43(2): 88–90
12. Yamashita T, Qin G, Suzuki T, Ohishi Y. A new green fiber laser using terbium-doped fluoride fiber, in *Optical Fiber Communication Conference/National Fiber Optic Engineers Conference. OSA Technical Digest (CD)*. p. JWA18.
13. Amaranath G, Buddhudu S, Bryant FJ. Emission properties of Tb<sup>3+</sup>-doped alkali mixed fluoride glasses, *Solid State Commun.* 1989; 72(9): 923–925
14. Smart RG, Hanna DC, Tropper AC, Davey ST, Carter SF, Szebesta D. CW upconversion lasing at blue, green and red wavelengths in an infrared-pumped Pr<sup>3+</sup>-doped fluoride fibre at room temperature, *Electron Lett.* 1991; 27(14): 1307–1309
15. Zhang L, Xia Y, Shen X, Wei W. Concentration dependence of visible luminescence from Pr<sup>3+</sup>-doped phosphate glasses, *Spectrochim Acta A.* 2019; 206: 454–459
16. Zhang L, Peng M, Dong G, Qiu J. An investigation of the optical properties of Tb<sup>3+</sup>-doped phosphate glasses for green fiber laser, *Opt. Mater.* 2012; 34(7): 1202–1207
17. Baccaro S, Dall'Igna R, Fabeni P, Martini M, Mares JA, Meinardi F, et al. Ce<sup>3+</sup> or Tb<sup>3+</sup>-doped phosphate and silicate scintillating glasses, *J Lumin.* 2000; 87–89: 673–675
18. Takebe H, Nageno Y, Morinaga K. Compositional dependence of Judd–Ofelt parameters in silicate, borate, and phosphate glasses, *J Am Ceram Soc.* 1995; 78(5): 1161–1168
19. Pugliese D, Boetti NG, Lousteau J, Ceci-Ginistrelli E, Bertone E, Geobaldo F, et al. Concentration quenching in an Er-doped phosphate glass for compact optical lasers and amplifiers, *J Alloy Compd.* 2016;

657: 678–683

20. Hu L, He D, Chen H, Wang X, Meng T, Wen L, et al. Research and development of neodymium phosphate laser glass for high power laser application, *Opt Mater.* 2017; 63: 213–220
21. Guo J, Wang J, Wei H, Huang W, Huang T, Xia G, et al. High-power, Joule-class, temporally shaped multi-pass ring laser amplifier with two Nd:glass laser heads, *High Power Laser Sci Eng.* 2019; 7: e8
22. Lin H, Pun EY-B, Wang X, Liu X. Intense visible fluorescence and energy transfer in  $\text{Dy}^{3+}$ ,  $\text{Tb}^{3+}$ ,  $\text{Sm}^{3+}$  and  $\text{Eu}^{3+}$  doped rare-earth borate glasses, *J Alloy Compd.* 2005; 390(1): 197–201
23. Sun X-Y, Gu M, Huang S-M, Liu X-L, Liu B, Ni C. Enhancement of  $\text{Tb}^{3+}$  emission by non-radiative energy transfer from  $\text{Dy}^{3+}$  in silicate glass, *Physica B.* 2009; 404(1): 111–114
24. Ramachari D, Moorthy LR, Jayasankar CK. Energy transfer and photoluminescence properties of  $\text{Dy}^{3+}/\text{Tb}^{3+}$  co-doped oxyfluorosilicate glass–ceramics for solid-state white lighting, *Ceram Int.* 2014; 40(7, Part B): 11115–11121
25. Caldiño U, Muñoz H G, Camarillo I, Speghini A, Bettinelli M. Down-shifting by energy transfer in  $\text{Tb}^{3+}/\text{Dy}^{3+}$  co-doped zinc phosphate glasses, *J Lumin.* 2015; 161: 142–146
26. Sobha KC, Rao KJ. Luminescence of, and energy transfer between  $\text{Dy}^{3+}$  and  $\text{Tb}^{3+}$  in NASICON-type phosphate glasses, *J. Phys. Chem. Solids.* 1996; 57(9): 1263–1267
27. Juárez-Batalla J, Meza-Rocha AN, Muñoz H G, Caldiño U. Green to white tunable light emitting phosphors:  $\text{Dy}^{3+}/\text{Tb}^{3+}$  in zinc phosphate glasses, *Opt. Mater.* 2017; 64: 33–39
28. Stachurski ZH, Fundamentals of amorphous solids: structure and properties. Wiley-VCH , Higher Education Press, 2015.
29. Ofelt GS. Intensities of crystal spectra of rare-earth ions, *J Chem Phys.* 1962; 37(3): 511–520
30. Judd BR. Optical absorption intensities of rare-earth ions, *Phys Rev.* 1962; 127(3): 750–761
31. Carnall WT, Fields PR, Rajnak KJ. Electronic energy levels of the trivalent lanthanide aquo ions. III.  $\text{Tb}^{3+}$ , *J Chem Phys.* 1968; 49(10): 4447–4449
32. Jamalaiah BC, Suresh Kumar J, Mohan Babu A, Sasikala T, Rama Moorthy L. Study on spectroscopic and fluorescence properties of  $\text{Tb}^{3+}$ -doped LBTAf glasses, *Physica B.* 2009; 404(14): 2020–2024
33. Jamalaiah BC, Vijaya Kumar MV, Rama Gopal K. Investigation on luminescence and energy transfer in  $\text{Tb}^{3+}$ -doped lead telluroborate glasses, *Physica B.* 2011; 406(14): 2871–2875
34. Bindu SH, Raju DS, Krishna VV, Raju CL, Preparation and characterization of  $\text{Tb}^{3+}$  ions doped zincborophosphate glasses for green emission, in *AIP Conference Proceedings*. Vol. 1849. p. 020002.
35. Amaranath G, Buddhu S, Bryant FJ. Spectroscopic properties of  $\text{Tb}^{3+}$ -doped fluoride glasses, *J Non-Cryst Solids.* 1990; 122(1): 66–73
36. Dornauf H, Heber J. Concentration-dependent fluorescence-quenching in  $\text{La}_{1-x}\text{Pr}_x\text{P}_5\text{O}_{14}$ , *J. Lumin.* 1980; 22(1): 1–16
37. Reddy Prasad V, Babu S, Ratnakaram YC. Concentration dependent luminescence properties of  $\text{Dy}^{3+}$ -doped lead free zinc phosphate glasses for visible applications, *Indian J. Phys.* 2016; 90(10): 1173–1182
38. M.Vijayakumar, K.Viswanathan, K.Marimuthu. Structural and optical studies on  $\text{Dy}^{3+}:\text{Tb}^{3+}$  co-doped zinc leadfluoro-borophosphate glasses for white light applications, *J Alloy Compd.* 2018; 745: 306–318
39. Velázquez JJ, Rodríguez VD, Yanes AC, delCastillo J, MéndezRamos J. Increase in the  $\text{Tb}^{3+}$  green emission in  $\text{SiO}_2\text{-LaF}_3$  nano-glass-ceramics by codoping with  $\text{Dy}^{3+}$  ions, *J Appl Phys.* 2010; 108(11): 628
40. Zur L, Kos A, Górny A, Sołtys M, Pietrasik E, Pisarska J, et al. Influence of acceptor concentration on crystallization behavior and luminescence properties of lead borate glasses co-doped with  $\text{Dy}^{3+}$  and  $\text{Tb}^{3+}$  ions, *J Alloy Compd.* 2018; 749: 561–566

41. Sun XY, Yu XG, Jiang DG, Wang WF, Li YN, Chen ZQ, et al. Spectroscopic and energy transfer properties of Dy<sup>3+</sup>-doped, Tb<sup>3+</sup>/Dy<sup>3+</sup>-codoped dense oxyfluoride borogermanate scintillating glasses, J Appl Phys. 2016; 119(23): 233103.233101-233103.233108
42. Dexter DL. A theory of sensitized luminescence in solids, J Chem Phys. 1953; 21(5): 836-850
43. Reisfeld R, Greenberg E, Velapoldi R, Barnett B. Luminescence quantum efficiency of Gd and Tb in borate glasses and the mechanism of energy transfer between them, J Chem Phys. 1972; 56(4): 1698-1705